Inter-Domain Redox Communication in Flavoenzymes of the Quiescin/Sulfhydryl Oxidase Family: Role of a Thioredoxin Domain in Disulfide Bond Formation[†,‡]

Sonali Raje and Colin Thorpe*

Department of Chemistry and Biochemistry, University of Delaware, Newark Delaware 19716

Received January 3, 2003; Revised Manuscript Received February 25, 2003

ABSTRACT: Flavoproteins of the quiescin/sulfhydryl oxidase (QSOX) family catalyze oxidation of peptide and protein thiols to disulfides with the reduction of oxygen to hydrogen peroxide. QSOX family members contain several domains, including an N-terminal thioredoxin domain (Trx) and an FAD-binding-domain (ERV) toward the C-terminus. Partial proteolysis of avian QSOX leads to two fragments, designated 30 and 60 kDa from their apparent mobilities on SDS−PAGE. The 30 kDa fragment is a monomer under nondenaturing conditions and contains a Trx domain with a CxxC sequence typical of protein disulfide isomerase (WCGHC). This QSOX fragment is not detectably glycosylated, contains no detectable FAD, and shows undetectable sulfhydryl oxidase activity. In contrast, the 60 kDa fragment is a dimeric glycoprotein that binds FAD tightly and oxidizes dithiothreitol about 1000-fold slower than intact QSOX. Reduced RNase is not a significant substrate of the 60 kDa fragment. The redox behavior of the 60 kDa flavoprotein fragment is profoundly different from that of intact QSOX. Thus, dithionite or photochemical reduction of the 60 kDa fragment leads to two-electron reduction of the FAD without subsequent reduction of the other two CxxC motifs or the appearance of a thiolate to flavin charge-transfer complex. Further characterization of the fragments and insights gained from the crystal structure of yeast ERV2p (Gross, E., Sevier, C. S., Vala, A., Kaiser, C. A., and Fass, D. (2002) *Nat. Struct. Biol. 9,* 61−67) suggest that the flow of reducing equivalents in intact avian QSOX is dithiol substrate → C80/83 → C519/522 → C459/462 → FAD → oxygen. The ancient fusion of thioredoxin domains to a catalytically more limited ERV domain has produced an efficient catalyst for the direct introduction of disulfide bonds into a wide range of proteins and peptides in multicellular organisms.

Avian, human, and rat FAD-dependent sulfhydryl oxidases (*1*, *2*) have been recently recognized as founding members of a new family of enzymes present in all multicellular organisms. They catalyze formation of disulfide bonds, with the reduction of molecular oxygen to hydrogen peroxide:

$$2\ R{-}SH + O_2 \rightarrow R{-}S{-}S{-}R + H_2O_2$$

The avian oxidase, the best characterized enzymologically (*1*, *3*−*8*), catalyzes the facile, direct insertion of disulfide bonds into a range of peptides and proteins. Providing that the cysteine-containing substrate is conformationally mobile, there appears little dependence of catalytic parameters on molecular weight or isoelectric point. The avian enzyme cooperates with PDI[1] to rapidly generate the correct disulfide pairings in RNase A. Expression and distribution patterns of the rat and human FAD-dependent sulfhydryl oxidases suggest that they are particularly abundant in tissues that are heavily involved in the secretion of disulfide-rich peptides and proteins (*2*, *8*−*10*).

Our initial mechanistic work on the avian oxidase relied heavily on the precedents set by enzymes of the pyridine nucleotide-disulfide oxidoreductase family (*11*) because it was also found to contain both an FAD prosthetic group and a redox active disulfide bridge (*5*). The two-electron reduced enzyme (E_{2e}; Scheme 1) is an equilibrium mixture between a form showing a prominent thiolate to oxidized flavin charge-transfer complex (E_{2e}^{A}) and a species in which the two electrons are on the isoalloxazine ring (E_{2e}^{B}). Equilibration between these two forms appeared, somewhat surprisingly, to be rate limiting with good thiol substrates (*7*). As expected, the addition of two more electrons to the E_{2e} species yields the E_{4e} state (Scheme 1).

A minimal chemical mechanism for the avian enzyme, incorporating results from static and rapid reaction studies (*4*, *7*), was proposed before the amino acid sequence of the protein became available. Surprisingly, the sequence of the avian enzyme, and its homologues, shows three, not one, −CxxC− motifs in a protein formed from the fusion of two ancient gene families (*1*, *2*, *8*, *12*). This fusion was originally recognized in a protein, Quiescin Q6, that was differentially expressed as human fibroblasts enter quiescence (*12*, *13*). Quiescin/sulfhydryl oxidase (QSOX) homologues are found in protists, plants, and metazoans (*1*, *2*, *8*). The domain structure of QSOX and the complete amino acid sequence

[†] This work was supported by NIH Grant GM26643.

[‡] This work is dedicated to the memory of the late Professor Vincent Massey.

* Author for correspondence. Phone: (302) 831-2689. Fax: (302) 831-6335. E-mail: cthorpe@udel.edu.

[1] Abbreviations: ALR, augmenter of liver regeneration; DTT, dithiothreitol; ERV, protein essential for respiration and viability in yeast; GSH, reduced glutathione; NEM, *N*-ethyl maleimide; PDI, protein disulfide isomerase; PVDF, polyvinylidene fluoride; QSOX, flavin-dependent sulfhydryl oxidases homologous to Quiescin Q6; Trx, thioredoxin; TrxR, thioredoxin reductase; NADPH, reduced nicotinamide adenine dinucleotide phosphate.

10.1021/bi030003z CCC: $25.00
Published on Web 03/27/2003

Scheme 1: Initial Model of Redox States in Avian Sulfhydryl Oxidase[a]

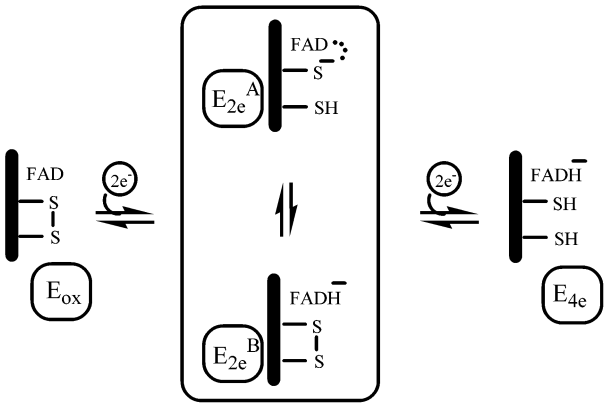

[a] The protonation state of the reduced flavin is not yet known.

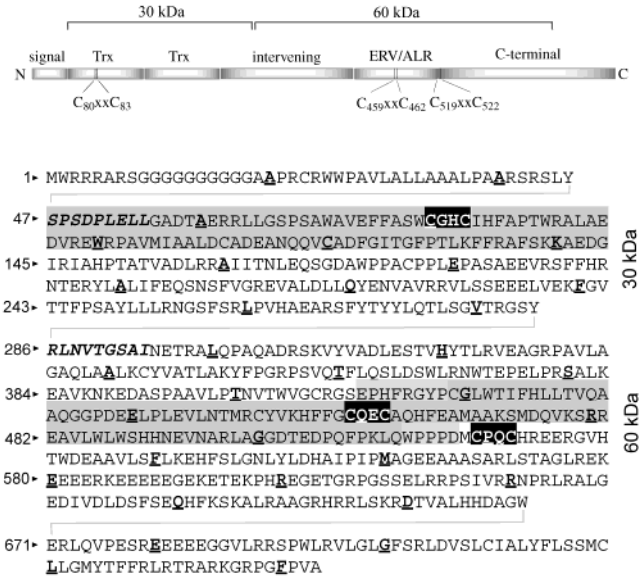

FIGURE 1: Domain structure and amino acid sequence of avian QSOX. Top: the thioredoxin and ALR/ERV domains are drawn approximately to scale within the 743 amino acid polypeptide predicted from the DNA sequence of avian QSOX. Bottom: amino acid sequence of avian QSOX. The first thioredoxin domain (Trx) and the ERV/ALR domain are shaded. The three CxxC motifs are bolded against a black background. The bolded, italicized, sequences (S_{47}PS− and R_{286}LN−) represent the N-termini of 30 and 60 kDa fragments, respectively. For clarity, these proteolytic fragments are separated within the sequence. Every 20th amino acid is bolded and underlined. The first amino acid of alternate lines of sequence is numbered.

of the avian enzyme are shown in the upper and lower sections of Figure 1, respectively.

Toward the N-terminus of QSOX are two thioredoxin (Trx) domains. The first is readily identified in standard database searches and contains the W**C**GH**C** (C80/83) motif found in protein disulfide isomerase (PDI; Figure 1). A second Trx domain shows weaker similarity to thioredoxin sequences and lacks a potential redox-active disulfide (Figure 1). Next comes an intervening sequence, without obvious homology to proteins outside the QSOX family (*8*), and then follows a domain defined by the ERV/ALR family. ERV1p, ERV2p, and ALR have been shown by Lisowsky and co-workers (*14*−*18*) and Kaiser and colleagues (*19*, *20*) to be diminutive stand-alone FAD-dependent sulfhydryl oxidases with a wide range of apparent cellular roles. A recent crystal structure of ERV2p by Fass and co-workers shows a single domain containing about 110 residues in a distorted 4-helix bundle (*19*). The redox-active CxxC motif corresponding to that identified by Hoober et al. (C459/462 in avian QSOX; Figure 1; *1*) is adjacent to the re-face of the isoalloxazine ring. Of these cysteines, C462 is perfectly positioned for subsequent C-4a adduct formation (*11*, *19*). A third CxxC motif (C519/522) occurs close to the junction between the ERV/ALR domain and a variable C-terminal region (*8*).

Since we have yet to express active, full-length, recombinant QSOX, we have utilized partial proteolysis of the egg-white protein to prepare and characterize folded fragments of this rather large glycosylated enzyme. We show that removal of the N-terminal thioredoxin domains has profound effects on the redox behavior and catalytic activity of QSOX. The data presented here suggest that all three CxxC motifs are required for the efficient oxidation of thiol substrates by this versatile catalyst of protein disulfide bond formation (*6*−*8*).

MATERIALS AND METHODS

Materials. Purified chicken egg-white sulfhydryl oxidase was a gift from Dr. Karen Hoober. Thioredoxin and thioredoxin reductase were generously provided by Dr. Charles Williams. Methyldiiodoarsine was synthesized by Mr. Dan Cline as described earlier (*21*) and rapidly hydrolyzes to the methylarsonous species when added to aqueous buffers (*22*). RNase, DTT, NADPH, GSH, TFA, chymotrypsin, trypsin, and thermolysin were obtained from Sigma. Sequencing-grade endoproteinase LysC was obtained from Promega. Acetonitrile was from Fisher Scientific. Sinapinic acid was purchased from Aldrich. Superdex-200 gel filtration and Phenyl Superose HR 10/10 columns were from Pharmacia Biotech. Immobilon-P electroblotting membranes were obtained from Millipore. SDS−PAGE gels (4−15% and 18% Tris-HCl) were purchased from Bio-Rad.

General Methods. Visible and ultraviolet spectra were recorded on a Hewlett-Packard 8452A instrument. Egg-white sulfhydryl oxidase concentrations are reported with respect to enzyme-bound flavin using a molar extinction coefficient of 12.5 mM^{-1} cm^{-1} at 454 nm (*5*). The molar extinction coefficient for the 60 kDa fragment was determined to be 12.5 mM^{-1} cm^{-1} by following the release of the bound flavin in 0.1% SDS. The extinction coefficient for the 30kDa fragment was calculated to be 37.6 mM^{-1} cm^{-1} at 280 nm using the ProtParam tool located on the ExPASy Molecular Biology Server. The molar extinction coefficients for NADPH, thioredoxin, and thioredoxin reductase were 6.2, 12.7, and 11.3 mM^{-1} cm^{-1} at 340, 280, and 458 nm respectively. Oxygen electrode assays utilized a Clark type (YSI 5331) instrument using 5 mM DTT in 3 mL of 50 mM air-saturated potassium phosphate buffer pH 7.5 (*5*). Fluorescence measurements used an SLM-Aminco Bowman Series 2 luminescence spectrometer. Fluorescence microcell assays used 300 μM thiols, from either DTT or reduced RNase, following the peroxidase-mediated oxidation of homovanillic acid (*23*). Anaerobic procedures, using all-glass titration cuvettes, were as described earlier (*24*). The 60 kDa fragment was photoreduced at 4 °C in an anaerobic cuvette 4 cm from a 150 W flood lamp using 1 μM 5-deazaflavin and 1 mM EDTA

essentially as described earlier (*5*). In-gel glycoprotein staining used a GelCode Glycoprotein Staining Kit from Pierce. Enzymatic deglycosylation of full-length protein and of the 60kDa fragment followed the procedure outlined in the GLYKO kit.

Trial digestion of sulfhydryl oxidase used trypsin and chymotrypsin in 50 mM ammonium bicarbonate buffer, 0.3 mM EDTA, at pH 8.0; thermolysin in 50 mM Tris pH 8.0; and sequencing grade endoproteinase LysC with 25 mM TrisHCl, 0.3mM EDTA, pH 9.2.

Digestion of Sulfhydryl Oxidase. Sulfhydryl oxidase (110 μg) was digested at 37 °C with 0.5% (w/w) α-chymotrypsin (bovine pancreas type II; triple crystallized) in 50 μL of 50 mM ammonium bicarbonate buffer, pH 8.0, containing 0.3 mM EDTA. Aliquots (10 μL) of the digest were withdrawn at 2, 3, 4, 10, and 30 min, mixed with 10 μL of 2× Laemmli buffer, and placed in a boiling water bath for 5 min. Samples were analyzed using 12.5% SDS−PAGE gels with Coomassie staining.

Purification of Sulfhydryl Oxidase Fragments. Sulfhydryl oxidase (1.3 mg) was digested as above in a total volume of 500 μL. After 25 min, the digest was brought to 43% saturation in ammonium sulfate and frozen immediately to retard further proteolysis. The thawed digest was immediately applied to a Phenyl-Sepharose HR10/10 column equilibrated with 43% saturated ammonium sulfate in 20 mM Tris buffer, pH 7.5, containing 0.3 mM EDTA. The column was developed at 1 mL/min with a linear decreasing gradient to 0% ammonium sulfate over 30 min, with an additional buffer wash for 20 min. The 60 and 30 kDa fragments eluted at 21 and 38 min, respectively. Traces of undigested QSOX eluted at 36 min. Where necessary, gel filtration on a Superdex 200 column equilibrated with 100 mM potassium phosphate buffer, pH 7.5, containing 0.3 mM EDTA and 100mM KCl (*4*), was used to completely remove residual undigested QSOX from the 30 kDa pool. Ovalbumin, cytochrome *c*, bovine serum albumin, carbonic anhydrase, aldolase, and thyroglobulin were used as molecular weight standards for gel filtration.

Sequence Analysis and Mass of Sulfhydryl Oxidase Fragments. Sulfhydryl oxidase was digested as above. The gel was then electroblotted (100 mA for 16 h at 4 °C) on an Immobilon-P membrane in 10 mM of 3-(cyclohexylamino)-1-propanesulfonate buffer containing 10% methanol, pH 11.0. Bands corresponding to the protein fragments of interest were excised and sequenced using an Applied Biosystems Procise Protein Sequencer equipped with an 140C microgradient system and a series 200 UV/VIS detector. Mass spectra were obtained using salt-free, lyophilized samples in 30% acetonitrile/0.1% TFA in a sinapinic acid matrix using a Bruker OmniFLEX MALDI-TOF spectrometer. RNase and bovine serum albumin were external standards.

RESULTS AND DISCUSSION

Partial Proteolysis of Avian Sulfhydryl Oxidase. Preliminary experiments were conducted by incubating the avian enzyme with 0.5% w/w chymotrypsin, trypsin, thermolysin, and LysC. Only chymotrypsin caused significant fragmentation of the native oxidase (data not shown). Figure 2 shows a time course of chymotrypsin treatment. The enzyme is heavily glycosylated (*5*) and runs as a diffuse band centered

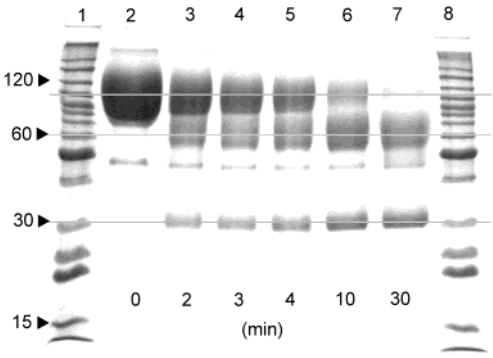

FIGURE 2: Partial proteolysis of avian sulfhydryl oxidase followed by SDS−PAGE. Lane 2 shows undigested sulfhydryl oxidase reduced with β-mercaptoethanol and run on SDS−PAGE. Lanes 3−7 correspond to 2, 3, 4, 10, and 30 min chymotrypsin treatment, respectively. Lanes 1 and 8 show the molecular weight markers.

at about 100 kDa in lane 2 of this SDS−PAGE gel. Lane 2 also shows that overloaded samples of native enzyme show a weak additional band at 48 kDa when the samples are boiled with β-ME. This slight contaminant does not influence the conclusions of this paper and is not present in the purified fragments described below. Under these conditions cleavage is half complete at about 2 min (not shown) and generates two bands corresponding to approximately 30 and 60 kDa. At 30 min, the native protein is almost entirely cleaved into the two fragments. The 30 kDa fragment migrates as a relatively compact band and shows no detectable staining for carbohydrate (see Methods). In contrast, the larger fragment runs as a diffuse band centered at about 60 kDa and remains heavily glycosylated. No other smaller fragments were evident using 12.5%, 18% gels, or 4−15% gradient gels. While essentially complete cleavage of the oxidase is observed after about 30 min (Figure 2), extending the incubation to 12 h leads to almost complete loss of the 60 kDa band without the appearance of fragments detectable in SDS−PAGE gels. The 30 kDa fragment appears somewhat more resistant to proteolysis under these conditions, with about 25% intensity remaining after 12 h.

Locating the 30 and 60 kDa Fragments within the Full-Length Sequence. Electroblotting onto PVDF-membranes followed by gas-phase protein sequencing showed N-terminii of S_{47}PSDPLELL− and R_{286}LNVTGSAI− for the 30 and 60 kDa fragments, respectively. Both N-terminii (bolded and italicized in Figure 1) follow a tyrosine residue in the sequence, consistent with a typical chymotrypsin cleavage pattern. The 30 kDa fragment starts close to the N-terminus of the mature avian sulfhydryl oxidase, just inside the first thioredoxin motif (shaded in Figure 1; see Discussion). MALDI of this 30 kDa apparently non- or lightly glycosylated fragment gave a mass of 29.1 kDa (not shown, see Methods), consistent with the SDS−PAGE result. However the calculated mass of a 239 residue fragment starting at the identified N-terminus (S_{47}PSD) and ending at the cleavage between the two fragments (R_{282}GSY, Figure 1) is somewhat smaller (26.7 kDa). The difference might reflect unidentified posttranslational modification of the fragment, but this does not affect the arguments made later in the paper. The 30 kDa fragment contains numerous potential chymotrypsin sites, and thus its comparative resistance to proteolysis suggests a module of substantially ordered structure.

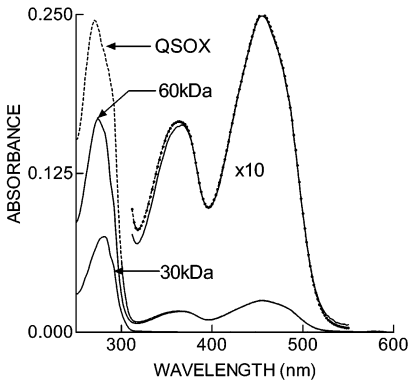

FIGURE 3: UV−vis spectra of native QSOX and 30 and 60 kDa fragments. Spectra were recorded in 50 mM potassium phosphate buffer, containing 0.3 mM EDTA, pH 7.5. Equimolar concentrations (2 μM) of the intact enzyme and the fragments were used.

The 60 kDa fragment was deglycosylated under denaturing conditions and gave a sharper band at 45 kDa (not shown; see Methods), suggesting that this fragment extends to about residue 670 ($HDAGW_{670}$). Clearly, the 60 kDa glycosylated fragment includes an N-terminal region of about 125 residues, the approximately 105 residue ALR/ERV domain (*19*), and finally about 150 residues to the C-terminus. Close to the junction of the ALR/ERV domain and the C-terminal section is a third CxxC motif (CPQC; highlighted in Figure 1; see later). Overall, the 60 kDa piece contains a total of eight cysteine residues (including two CxxC motifs). The 30 kDa fragment contains five cysteine residues including the WCGHC motif typical of an active-site disulfide in PDI. We next show that the 30- and 60 kDa fragments are readily separable under nondenaturing conditions without prior reduction of disulfide bonds.

Chromatographic Separation of 30- and 60 kDa Fragments. An excellent separation between 30 and 60 kDa fragments was obtained using hydrophobic interaction chromatography (see Methods). The 60 kDa glycosylated piece emerged first, well-separated from the 30 kDa fragment and any uncut sulfhydryl oxidase. To make certain that the smaller fragment was completely freed from intact QSOX, an additional gel filtration step was employed (see Methods). This was critically important when the enzymatic activity of the fragment (in isolation or in combination) was assessed. Using a calibrated gel filtration column the 30 and 60 kDa fragments showed apparent native molecular weights in 100 mM phosphate buffer containing 100 mM KCl (*4*) of 29 kDa and about 150 kDa, respectively. Thus, the 30 kDa piece is clearly monomeric. The larger fragment is probably a dimer under these conditions, consistent with prior results from the intact enzyme (*5*) and with the suggested flow of reducing equivalents in ERV2p (*19*; see later).

Spectrophotometric Characterization of 30 and 60 kDa Fragments. The UV−vis spectrum of the monomeric 30 kDa fragment shows undetectable flavin absorbance (Figure 3). In contrast, the 60 kDa piece shows a visible spectrum almost coincident with that of the native oxidase (with an essentially identical extinction coefficient for bound FAD of 12. 5 $mM^{-1}cm^{-1}$; Figure 3, see Methods). The segregation of the FAD with the 60 kDa piece is consistent with the location of the ERV/ALR domain within this fragment. As expected, the protein/flavin absorbance ratio (280/454 nm) for the 60 kDa fragment is smaller than that for the native oxidase (6.4 vs 9.8). Further, the difference spectrum (native oxidase, 60 kDa fragment) closely approximates the spectrum of the isolated 30 kDa piece (not shown). These data suggest that there is no major change in the environment of the flavin cofactor on fragmentation of the protein.

Enzymatic Activity of 30 and 60 kD Fragments of Avian QSOX. The pure 30 kDa fragment showed undetectable activity toward DTT in either the standard oxygen electrode assay, the discontinuous DTNB assay or a sensitive new fluorescence assay using homovanillic acid (see Methods; *3*, *4*, *23*). This is to be expected, since it lacks the FAD binding domain of the native protein.

In contrast, the 60 kDa piece retains significant sulfhydryl oxidase activity using DTT. The most obvious difference is that instead of k_{cat} and K_m values of 1030 min^{-1} and 0.14 mM DTT shown by the native protein (*4*, *6*), the fragment shows an essentially linear dependence of rate up to 12.5 mM DTT (data not shown). This is consistent with a very large K_m value for DTT. Comparing activities at 0.14 mM DTT (the K_m for QSOX), the 60 kDa fragment is some 1000-fold slower than QSOX. Rate measurements for the fragment used 1 μM bound FAD in the oxygen electrode. Since free flavins can show significant nonenzymatic reduction with thiols (with consequent oxygen consumption in aerobic solution), control experiments were performed with 1 μM free FAD. No significant rate was observed up to 12.5 mM DTT (not shown). Thus, the DTT oxidase activity of the 60 kDa fragment, while small, is real. In contrast, the fragment shows no measurable oxidation of reduced RNase (at 460 μM thiol: about 4-fold higher than the K_m observed for the native oxidase; *3*, *4*, *6*). In sum, these data suggest that communication between 30 and 60 kDa is very important for the catalytic efficiency of the holoenzyme. Reductive titrations and pre-steady-state kinetics of the 60 kDa domain confirm and extend this conclusion.

Anaerobic Spectrophotometric Experiments with the 60 kDa Fragment. Striking differences in the redox behavior between the fragment and intact QSOX are evident from anaerobic experiments. For context, it is first necessary to consider the behavior of the native enzyme. Two electron reduction of the native enzyme gives a distinct thiolate to FAD charge-transfer complex at pH 7.5 (inset to Figure 4; *4*). Previous static experiments have shown that the intensity of this band is the same, whether it is generated on reduction (using dithionite titrations or light/deazaflavin) or upon reoxidation of E_{4e} (with ferricyanide). This is because equilibrium between $E_{2e}{}^A$ and $E_{2e}{}^B$ (Scheme 1) is attained during these static experiments. The addition of a further two electrons fully reduces the flavin to generate the E_{4e} state shown in Scheme 1 (*4*). However, a further four electrons can be delivered to the enzyme, with reduction of the two additional CxxC motifs, but this does not lead to significant changes in the visible region of the spectrum (see later).

In sharp contrast to intact QSOX, the 60 kDa fragment reproducibly requires only two (not four) electrons for full reduction of the FAD moiety (as in the dithionite titration of Figure 4, panel B). This seemed surprising, since the 60 kDa fragment contains not only FAD but also two CxxC motifs (C459/462 and C519/522). The first of these disulfides is the one originally identified as the redox-active disulfide in intact QSOX (*1*) and corresponds to C121/124 in ERV2p (*8*, *19*). The C-terminal cysteine of this redox active disulfide

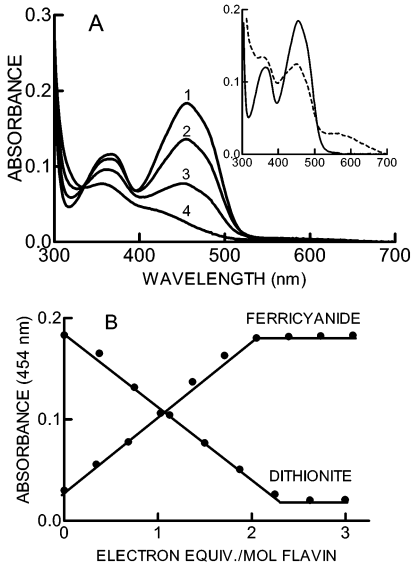

FIGURE 4: Dithionite titration of 60 kDa QSOX fragment. In panel A, curves 1−4 represent additions of 0, 0.75, 1.49, and 2.25 electron equiv/mol flavin, respectively. The inset shows the charge-transfer long-wavelength band for intact QSOX observed on two-electron reduction. Panel B shows absorbance changes at 454 nm during reduction of the 60 kDa fragment with dithionite and reoxidation with potassium ferricyanide.

lies against the isoalloxazine ring in the crystal structure of ERV2p (*19*) and is perfectly positioned for C-4a adduct formation (*11*, *25*). Why, then, do we see neither a charge-transfer complex, analogous to the one shown by QSOX, nor the uptake of at least 4-electrons on dithionite titration of the 60 kDa fragment? Additionally, the 60 kDa fragment retains the C519/522 disulfide lying at the junction between the ERV/ALR domain and the C-terminal region of QSOX (and in principle could take up a total of 6-electrons; see later).

Midway through the two-electron reduction of the 60 kDa fragment by dithionite (Figure 4A, main panel), small amounts of long wavelength absorbance are observed (e.g., at 580 nm, as seen in curves 2 and 3). Expansion of the absorbance axis (not shown) clearly shows this feature represents a blue semiquinone, and not the charge-transfer complex observed with QSOX. If it were a charge-transfer band (equivalent to E_{2e}^{A} for the uncut enzyme; Scheme 1), it would be expected to be seen, in an equilibrium amount, in both reduction and reoxidation phases of Figure 4. In fact, the long-wavelength feature is undetectable (not shown) during back-titration with two molecules of ferricyanide (panel B, Figure 4). This blue semiquinone is therefore kinetically stabilized and does not represent a comproportionation equilibrium. Dithionite titration of the fragment at pH 9.0 still showed no evidence of charge transfer absorbance. Instead, a substantial red, anionic, semiquinone feature is clearly observed after the addition of one electron per flavin (apparent molar absorbtivity 12 $mM^{-1}cm^{-1}$ at 372 nm; not shown).

In addition to dithionite titrations, we tried photoreduction (see Methods) of the 60 kDa fragment with 5-deazaflavin in an attempt to drive formation of four- or six-electron reduced enzyme. During this photoreduction (e.g., curve 2 in Figure 5), neither radical nor charge transfer bands were observed at pH 7.5. The reduced enzyme (apparently

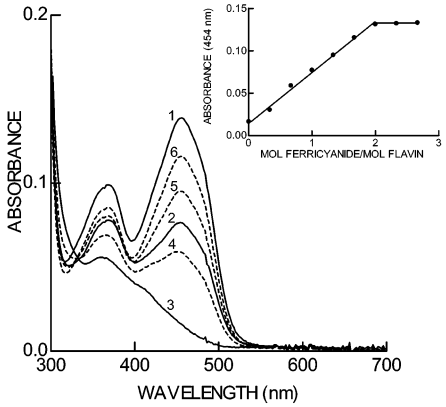

FIGURE 5: Photoreduction of 60 kDa fragment of QSOX and back-titration with ferricyanide. Curves 1 is the fully oxidized 60kDa fragment before 5-deazaflavin photoreduction (see Methods). Curves 2 and 3 show the enzyme after 3.9 and 61 min photoreduction. Intermittent spectra are omitted for clarity. Curves 4, 5, and 6 show the addition of 0.66, 1.33, and 1.66 mol ferricyanide/mol flavin, respectively. The inset plots absorbance changes during the ferricyanide back-titration.

completely formed after 7 min of illumination; not shown) was then subject to an additional 54 min of photoreduction (curve 3; see Methods) in the hope of driving further reduction of the enzyme. However, back-titration with anaerobic ferricyanide required the removal of only two electrons for reoxidation of the fragment (see inset). As before, no long-wavelength band was observed during the reoxidative phase of this experiment (dotted lines 4, 5, and 6).

We were finally successful at diverting electrons from dihydroflavin into a disulfide center of the 60 kDa fragment using alkylation with *N*-ethylmaleimide, or via reaction with diiodomonomethylarsenic(III), as described below. First, after dithionite reduction of the 60 kDa fragment to the two-electron reduced state (Figure 6, panel A, curve 2), NEM was tipped into the main-space of the anaerobic cuvette to a final concentration of 500 μM. A slow reoxidation of the flavin chromophore within the fragment was observed ($t_{1/2}$ of 27 min; panel B) with a final spectrum (curve 3) that is 4 nm blue-shifted from that seen for the original oxidized fragment (curve 1). While we do not yet know which cysteine residue or residues are targets of NEM, it is clear that alkylation promotes transfer of two-electrons from flavin with the net reduction of one disulfide bond in the 60 kDa fragment. Subsequent rereduction with dithionite (panel C) leads to an uptake of four more electrons, for an overall total of six electrons. Thus, alkylation enables the eventual reduction of FAD and both CxxC motifs in the 60 kDa fragment.

Arsenic (III) compounds have been widely used to probe redox catalysis in the pyridine nucleotide-disulfide oxidoreductase family and we therefore evaluated the effect of methylarsonous acid ($CH_3As(OH)_2$; As(III); see Materials and Methods (*21*, *22*) on the 60 kDa fragment. The rapid two-electron reduction of the 60 kDa fragment, in the presence of As(III), is followed by reoxidation of the enzyme FAD (half complete in about 1 h; Figure 7, curves 1 and 2, respectively). This reoxidized species (curve 2) was then mixed aerobically with 1 mM DTT. This dithiol binds arsenic(III) species tightly (*26*) regenerating active, truncated, enzyme (Figure 7, curve 3). As expected, the sulfhydryl oxidase activity of the fragment then depletes dissolved

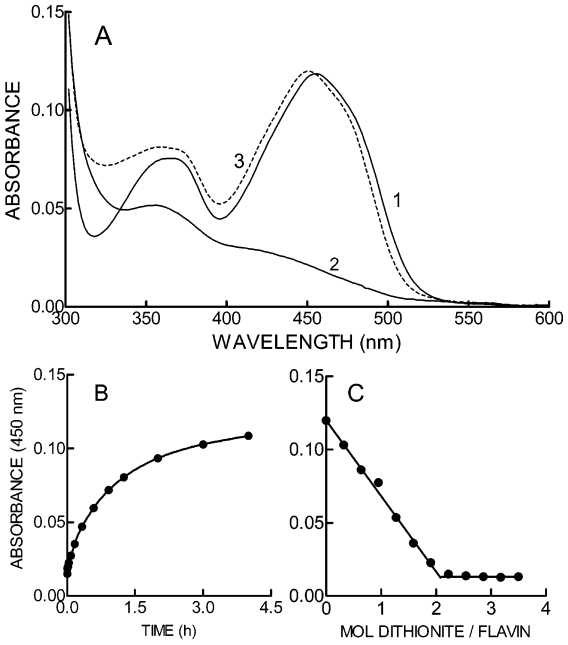

FIGURE 6: Preparation and redox behavior of an NEM-alkylated 60 kDa QSOX fragment. In panel A, curve 1 shows the oxidized 60kDa fragment after anaerobiosis. Curve 2 represents the fully reduced enzyme with 1.2 mol dithionite/mol flavin. NEM (500 μM) was then tipped from a sidearm, and the blue-shifted oxidized flavin spectrum shown in curve 3 reappeared slowly (panel B). Panel C plots the absorbance change for the subsequent titration of the alkylated 60 kDa fragment with standardized dithionite.

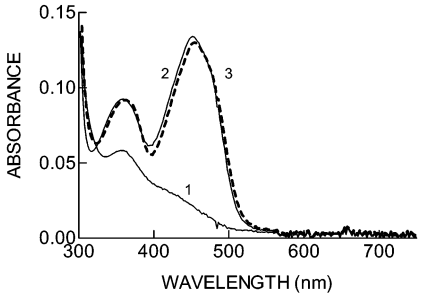

FIGURE 7: Labeling of the redox active disulfide bridge of the 60 kDa fragment with arsenic(III). The fragment (10.6 μM), in the presence of 60 μM di-iodomonomethyl arsenic (III), was made anaerobic and rapidly brought to the 2-electron-reduced state with dithionite (curve 1). A slow reappearance of the oxidized flavin yielded curve 2 (see text), and after opening the cuvette to air, the addition of 1 mM DTT immediately gave spectrum 3.

oxygen in solution followed by DTT-mediated bleaching of the flavin spectrum (not shown). Thus reversible ligation of vicinal thiols with As(III) can also perturb the internal redox equilibrium in the 60 kDa fragment. Arsenic binding, like alkylation, leads to a blue shift in the oxidized flavin absorbance envelope, as seen with lipoamide dehydrogenase on derivatization of the redox active disulfide bridge (*11*, *27*).

In aggregate, these data show that the equilibrium position for the two-electron reduced 60 kDa fragment lies far toward E_{2e}^{B} (Scheme 1) and that chemical trapping of the E_{2e}^{A} form is slow. Since photoreduction delivers reducing equivalents only to oxidized flavin in the E_{2e}^{A} form, very sluggish further reduction of the 60 kDa fragment would be expected. Later, we address possible reasons for this profound difference between intact enzyme and 60 kDa fragment.

The 30 kDa Fragment is a Substrate of the 60 kDa Fragment. The simplest explanation for the drastic decrease

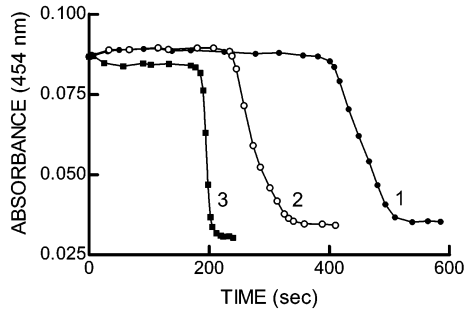

FIGURE 8: The 30 kDa fragment as a substrate of the 60 kDa fragment. Curve 1 represents absorbance changes at 454 nm for 6 μM of the 60 kDa fragment in the presence of 1 mM DTT. Curves 2 and 3 represent absorbance changes under identical conditions including 6 and 12 μM of the 30kDa fragment.

in catalytic activity on partial proteolysis is that the thioredoxin CxxC motif is the primary conduit for reducing equivalents from both DTT and reduced RNase into intact QSOX. As might be expected, the isolated 30 kDa fragment, carefully freed of any contaminating uncut QSOX activity, accelerated the DTT-mediated bleaching of the flavin prosthetic group of the 60 kDa piece. Curve 1 of Figure 8 shows the absorbance change at 454 nm for 6 μM of the 60kDa fragment in the presence of 1mM DTT. The lag corresponds to the time required to remove dissolved oxygen from the solution. Increasing concentrations of the 30 kDa fragment significantly shortens the lag phase (curves 2 and 3).

Possible Role of the Third CxxC Motif in QSOX Catalysis. Key insights into the possible role of the third CxxC motif (C519/522) in QSOX catalysis come from the studies of Fass, Kaiser, and co-workers on the crystal structure and mechanism of yeast ERV2p (*19*). They suggest the following flow of reducing equivalents between the three redox centers in this small homo-dimeric enzyme:

$$\text{Dithiol substrate} \rightarrow (\text{C176/178})_{\text{subunit B}} \rightarrow (\text{C121/124})_{\text{subunit A}} \rightarrow \text{FAD}_{\text{subunit A}} \rightarrow \text{O}_2$$

Thus the CxC (C176/178) motif in one subunit (here B) of ERV2p accepts reducing equivalents from dithiol substrates, and transmits them across the subunit interface to C121/C124 and the FAD (both of the A subunit). Mutagenesis of either C176 or C178 abolishes ERV2p activity (*19*). By analogy, Gross et al. suggested that the third CxxC motif in QSOX (C519/522; Scheme 1) would occupy a comparable position to this catalytically essential disulfide in ERV2p (*19*). Consistent with its catalytic importance, the C519/522 disulfide is conserved in all known QSOX sequences (*8*).

A schematic model for the suggested flow of reducing equivalents in QSOX is shown in panel A of Figure 9. A thioredoxin domain (right) and the ERV/ALR domain (left) of the A subunit are shown, together with the C519/522 disulfide from the B subunit (dashed semicircle; middle). Overall the flow of reducing equivalents can be represented as

$$\text{Dithiol substrate} \rightarrow (\text{C80/83})_{\text{subunit A}} \rightarrow (\text{C519/522})_{\text{subunit B}} \rightarrow (\text{C459/462})_{\text{subunit A}} \rightarrow \text{FAD}_{\text{subunit A}} \rightarrow \text{O}_2$$

Reduction of QSOX Mediated by Thioredoxin Reductase. Earlier reductive titrations of intact QSOX utilized reagents

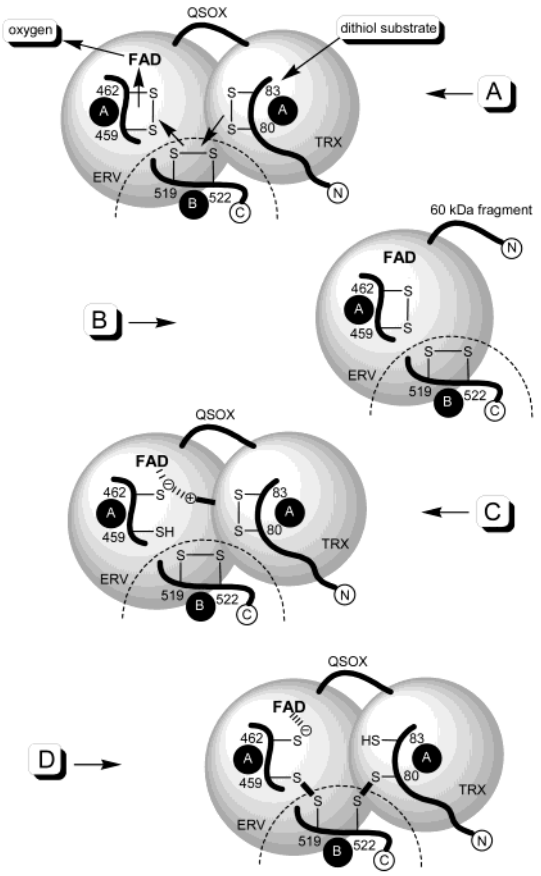

FIGURE 9: Schematic depiction of QSOX and 60 kDa fragment. Panel A shows the suggested flow of reducing equivalents from dithiol substrate to molecular oxygen. Small solid circles denote the A or B subunit of homodimeric avian QSOX. Panel B depicts the 60 kDa fragment. Panel C suggests stabilization of the charge-transfer thiolate via an interaction with the 30 kDa fragment. Panel D illustrates how inter-domain disulfide bond formation could contribute to stabilization of E_{2e}^{A}.

(e.g., dithionite or deazaflavin) which communicate via the flavin. Since reduced thioredoxin is a substrate of QSOX (*3*, *8*), an anaerobic experiment was conducted following the consumption of NADPH in the presence of catalytic levels of thioredoxin and its reductase as follows:

$$\text{NADPH} \rightarrow \text{TrxR} \rightarrow \text{Trx} \rightarrow \text{QSOX}$$

Spectra were recorded throughout the titration up to the addition of 4.6 mol of NADPH per mol of QSOX. Because of the overlap of spectral signals during the titration, Figure 10 depicts incremental difference spectra. Early in the titration, the difference spectrum 0.4−0.2 mol of NADPH (0.8−0.4 electrons; curve A) shows the expected accumulation of the charge-transfer spectrum of E_{2e}^{A}. After the E_{4e} state is passed (after 2 mol of NADPH), the flavin changes are essentially complete, leading to incremental difference spectrum (curve B; 3.1−2.9 mol of NADPH; 6.2−5.8 electrons) with neither subsequent changes in the flavin region, nor the accumulation of residual NADPH. However, when reduction of FAD and the three CxxC motifs is complete (at 4 mol of NADPH), the subsequent difference spectra show the stable accumulation of NADPH at 340 nm (curves C and D for 8.5−7.8 and 9.3−8.5 electrons respectively). This experiment, delivering electrons from a readily quantifiable titrant in the physiological direction,

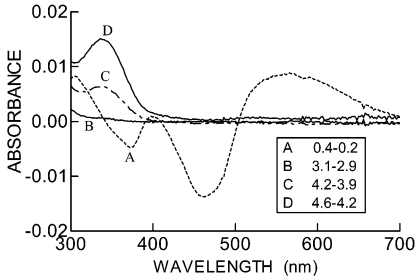

FIGURE 10: Difference spectra recorded during reduction of intact QSOX using NADPH, thioredoxin reductase and thioredoxin. QSOX (10 μM in the presence of 35 nM TrxR and 2 μM Trx) was titrated under anaerobic conditions with NADPH. Spectra were recorded after the changes were complete and selected difference spectra are presented to illustrate the progression of the titration. Curve A (0.4−0.2 mol NADPH) represents the initial part of the titration where the charge-transfer band is accumulating. Curves B, C, and D reflect difference spectra obtained after the addition of 3.1−2.9, 4.2−3.9, and 4.6−4.2 mol of NADPH respectively (see the text).

shows that QSOX can accept a total of about eight electrons. This is consistent with the model in Figure 9 and the arguments made above.

Role of Thioredoxin Domain in QSOX Catalysis. One striking finding of the present work is the drastic difference in redox behavior observed between intact QSOX and its 60 kDa fragment. Both are dimeric flavoproteins that have almost identical flavin spectra. Indeed, large differences in flavin environment between the two would not have been expected because the isoalloxazine ring is largely enclosed within the 4-helix bundle motif of ERV2p (*19*). However, the 60 kDa fragment (depicted in Figure 9B) stubbornly resists introduction of more than 2-electrons when the protein is reduced in the absence of chemical modification. Another significant difference is that the 60 kDa fragment does not form the thiolate (C462) to flavin charge-transfer complex so prominently observed in the 2-electron reduced state of QSOX (*4*, *7*).

Two rationalizations for these differences are presented in panels C and D of Figure 9. Both involve inter-domain interactions between 30 and 60 kDa fragments.

In panel C a favorable electrostatic attraction between C462 and the Trx domain is hypothesized, but any interaction which modulates the relative redox potentials of the participants would be relevant. One issue here is whether the 30 kDa fragment could approach the isoalloxazine and C459/462 moieties sufficiently closely when they are enclosed within the four-helix bundle of the ERV domain. A perhaps more likely explanation, is thermodynamic linkage via inter-domain disulfide bonds (panel D). Here the most oxidizing disulfide would be contributed by the thioredoxin domain. Indeed, this C80/83 disulfide sequence (WCGHC) resembles that of a typical protein disulfide isomerase and, as such, would be expected to be relatively oxidizing (*28*). The substantial reorganization of disulfides in panel D might also explain why the internal redox equilibration between flavin and disulfide moieties is surprisingly slow in avian QSOX catalysis (*7*).

Chains of interacting disulfides, as implied in panel D, have precedent in flavoprotein catalysis, e.g., in mercuric reductase (*29*), the high Mr forms of thioredoxin reductase (*30*) as well as the natural flavoprotein reductase/thioredoxin

fusions in *Mycobacterium leprae* (*31*), NADH oxidase from *Amphibacillus xylanus* (*32*), and in AhpF from *Salmonella typhimurium*. (*33*−*35*). The structure of AhpF suggests interesting parallels and contrasts with QSOX. AhpF has two contiguous thioredoxin domains toward the N-terminus of which only the second contains a CxxC motif (*34*). In QSOX, the first of two N-terminal thioredoxin domains is redox-active. The C-terminus of AhpF resembles thioredoxin reductase with an FAD and a second CxxC motif that can interact directly with the flavin (*34*). The 60 kDa domain of QSOX has an FAD binding domain, a second CxxC motif which lies directly next to the flavin and a third disulfide contributed by the other subunit (*8*, *19*).

The diminutive stand-alone flavoprotein sulfhydryl oxidases ERV2p and the viral ALR analogue, E10R, seem to be catalytic specialists, oxidizing reduced proteins through the mediation of PDI or a thioredoxin-like protein respectively (*8*, *14*, *20*, *36*). In contrast, QSOX appears to be a generalist, capable of directly and facilely oxidizing a wide range of reduced proteins and peptides without mediation of other proteins or small molecules (*6*, *8*). The natural fusion of thioredoxin and ERV domains has produced a highly versatile and efficient catalyst found in metazoans and plants that appears to have assumed the role played by ERV2p in yeast (*8*). A more detailed dissection of the catalytic functions of each domain in QSOX, and of the redox-active disulfide bonds housed within them, awaits the expression of recombinant protein.

ACKNOWLEDGMENT

We thank Drs. Karen Hoober and Charles Williams for gifts of materials, Dr.Yu-Chu Huang for N-terminal sequencing, and a referee for helpful comments.

REFERENCES

1. Hoober, K. L., Glynn, N. M., Burnside, J., Coppock, D. L., and Thorpe, C. (1999) Homology between egg white sulfhydryl oxidase and quiescin Q6 defines a new class of flavin-linked sulfhydryl oxidases, *J. Biol. Chem. 274*, 31759−31762.
2. Benayoun, B., Esnard-Fève, A., Castella, S., Courty, Y., and Esnard, F. (2001) Rat seminal vesicle FAD-dependent sulfhydryl oxidase: Biochemical characterization and molecular cloning of a member of the new sulfhydryl oxidase/quiescin Q6 gene family, *J. Biol. Chem. 276*, 13830−13837.
3. Hoober, K. L., and Thorpe, C. (2002) Flavin-dependent Sulfhydryl Oxidases in Protein Disulfide Bond Formation, *Methods Enzymol. 348*, 30−34.
4. Hoober, K. L. (1999) The isolation and initial characterization of a sulfhydryl oxidase from chicken egg white, PhD. Dissertation, University of Delaware, Newark, DE.
5. Hoober, K. L., Joneja, B., White, H. B., III., and Thorpe, C. (1996) A sulfhydryl oxidase from chicken egg white, *J. Biol. Chem. 271*, 30510−30516.
6. Hoober, K. L., Sheasley, S. S., Gilbert, H. F., and Thorpe, C. (1999) Sulfhydryl oxidase from egg white: a facile catalyst for disulfide bond formation in proteins and peptides, *J. Biol. Chem. 274*, 22147−22150.
7. Hoober, K. L., and Thorpe, C. (1999) Egg white sulfhydryl oxidase: Kinetic mechanism of the catalysis of disulfide bond formation, *Biochemistry 38*, 3211−3217.
8. Thorpe, C., Hoober, K. L., Raje, S., Glynn, N., Burnside, J., Turi, G., and Coppock, D. (2002) Sulfhydryl oxidases: emerging catalysts of protein disulfide bond formation in eukaryotes, *Arch. Biochem. Biophys. 405*, 1−12.
9. Musard, J. F., Sallot, M., Dulieu, P., Fraichard, A., Ordener, C., Remy-Martin, J. P., Jouvenot, M., and Adami, P. (2001) Identification and expression of a new sulfhydryl oxidase SOx-3 during the cell cycle and the estrus cycle in uterine cells, *Biochem. Biophys. Res. Commun. 287*, 83−91.
10. Ostrowski, M. C., and Kistler, W. S. (1980) Properties of a flavoprotein sulfhydryl oxidase from rat seminal vesicle secretion, *Biochemistry 19*, 2639−2645.
11. Williams, C. H., Jr. (1992) Lipoamide dehydrogenase, glutathione reductase, thioredoxin reductase, and mercuric ion reductase-A family of flavoenzyme transhydrogenases, in *Chemistry and Biochemistry of Flavoenzymes* (Müller, F., Ed.) Vol. III, pp 121−211, CRC Press, Boca Raton, FL.
12. Coppock, D. L., Cina-Poppe, D., and Gilleran, S. (1998) The Quiescin Q6 gene (QSCN6) is a fusion of two ancient gene families: thioredoxin and ERV1, *Genomics 54*, 460−468.
13. Coppock, D. L., Kopman, C., Scandalis, S., and Gillerman, S. (1993) Preferential gene expression in quiescent human lung fibroblasts, *Cell Growth Differ. 4*, 483−493.
14. Gerber, J., Muhlenhoff, U., Hofhaus, G., Lill, R., and Lisowsky, T. (2001) Yeast ERV2p is the first microsomal FAD-linked sulfhydryl oxidase of the Erv1p/Alrp protein family, *J. Biol. Chem. 276*, 23486-23491.
15. Lee, J., Hofhaus, G., and Lisowsky, T. (2000) Erv1p from Saccharomyces cerevisiae is a FAD-linked sulfhydryl oxidase, *FEBS Lett. 477* (*1*−*2*), 62−66.
16. Lisowsky, T., Lee, J. E., Polimeno, L., Francavilla, A., and Hofhaus, G. (2001) Mammalian augmenter of liver regeneration protein is a sulfhydryl oxidase, *Dig. Liver Dis. 33*, 173−180.
17. Lisowsky, T. (1992) Dual function of a new nuclear gene for oxidative phosphorylation and vegetative growth in yeast, *Mol. Gen. Genet. 232*, 58−64.
18. Lange, H., Lisowsky, T., Gerber, J., Muhlenhoff, U., Kispal, G., and Lill, R. (2001) An essential function of the mitochondrial sulfhydryl oxidase Erv1p/ALR in the maturation of cytosolic Fe/S proteins, *EMBO Rep 2*, 715−720.
19. Gross, E., Sevier, C. S., Vala, A., Kaiser, C. A., and Fass, D. (2002) A new FAD-binding fold and intersubunit disulfide shuttle in the thiol oxidase Erv2p, *Nat. Struct. Biol. 9*, 61−67.
20. Sevier, C. S., Cuozzo, J. W., Vala, A., Aslund, F., and Kaiser, C. A. (2001) A flavoprotein oxidase defines a new endoplasmic reticulum pathway for biosynthetic disulphide bond formation, *Nat. Cell Biol. 3*, 874−882.
21. Millar, I., Heaney, H., Heinekey, D., and Fernelius, W. (1960) *Inorg. Synth. 6*, 113−115.
22. Gailer, J., Madden, S., Cullen, W., and Denton, M. (1999) *Appl. Organomet. Chem. 13*, 837−843.
23. Raje, S., Glynn, N., and Thorpe, C. (2002) A continuous fluorescence assay for sulfhydryl oxidase, *Anal. Biochem. 307*, 266−272.
24. Williams, C. H., Arscott, L. D., Matthews, R. G., Thorpe, C., and Wilkinson, K. D. (1979) Methodology employed for anaerobic spectrophotometric titrations and for computer-assisted data analysis, *Methods Enzymol.* 185−198.
25. Thorpe, C., and Williams, C. H. (1976) Spectral Evidence for a Flavin Adduct in a Monoalkylated Derivative of Pig Heart Lipoamide Dehydrogenase, *J. Biol. Chem. 251*, 7726−7728.
26. Zahler, W. L., and Cleland, W. W. (1968) A specific and sensitive assay for disulfides, *J. Biol. Chem. 243*, 716−719.
27. Thorpe, C., and Williams, C. H., Jr. (1976) Differential reactivity of the two active site cysteine residues generated on reduction of pig heart lipoamide dehydrogenase, *J. Biol. Chem. 251*, 3553−3557.
28. Chivers, P. T., Prehoda, K. E., and Raines, R. T. (1997) The CXXC motif: a rheostat in the active site, *Biochemistry 36*, 4061−4066.
29. Miller, S. M., Moore, M. J., Massey, V., Williams, C. H., Jr., Distefano, M. D., Ballou, D. P., and Walsh, C. T. (1989) Evidence for the participation of Cys558 and Cys559 at the active site of mercuric reductase, *Biochemistry 28*, 1194−1205.
30. Williams, C. H., Arscott, L. D., Muller, S., Lennon, B. W., Ludwig, M. L., Wang, P. F., Veine, D. M., Becker, K., and Schirmer, R. H. (2000) Thioredoxin reductase two modes of catalysis have evolved, *Eur. J. Biochem. 267*, 6110−6117.
31. Wang, P. F., Marcinkeviciene, J., Williams, C. H., Jr., and Blanchard, J. S. (1998) Thioredoxin reductase-thioredoxin fusion enzyme from *Mycobacterium leprae*: comparison with the separately expressed thioredoxin reductase, *Biochemistry 37*, 16378−16389.
32. Ohnishi, K., Niimura, Y., Hidaka, M., Masaki, H., Suzuki, H., Uozumi, T., and Nishino, T. (1995) Role of cysteine 337 and

cysteine 340 in flavoprotein that functions as NADH oxidase from Amphibacillus xylanus studied by site-directed mutagenesis, *J. Biol. Chem. 270*, 5812−5817.
33. Poole, L. B. (1996) Flavin-dependent alkyl hydroperoxide reductase from *Salmonella typhimurium*. 2. Cystine disulfides involved in catalysis of peroxide reduction, *Biochemistry 35*, 65−75.
34. Wood, Z. A., Poole, L. B., and Karplus, P. A. (2001) Structure of intact AhpF reveals a mirrored thioredoxin-like active site and implies large domain rotations during catalysis, *Biochemistry 40*, 3900−3911.
35. Poole, L. B., Reynolds, C. M., Wood, Z. A., Karplus, P. A., Ellis, H. R., and Li Calzi, M. (2000) AhpF and other NADH: peroxiredoxin oxidoreductases, homologues of low Mr thioredoxin reductase, *Eur. J. Biochem. 267*, 6126−6133.
36. Senkevich, T. G., Weisberg, A. S., and Moss, B. (2000) Vaccinia virus E10R protein is associated with the membranes of intracellular mature virions and has a role in morphogenesis, *Virology 278*, 244−252.

BI030003Z